

# Multi-Modal MRI Reconstruction Assisted with Spatial Alignment Network

Kai Xuan, Lei Xiang, Xiaoqian Huang, Lichi Zhang, Shu Liao, Dinggang Shen\*, and Qian Wang\*

**Abstract**—In clinical practice, multi-modal magnetic resonance imaging (MRI) with different contrasts is usually acquired in a single study to assess different properties of the same region of interest in the human body. The whole acquisition process can be accelerated by having one or more modalities under-sampled in the  $k$ -space. Recent research has shown that, considering the redundancy between different modalities, a target MRI modality under-sampled in the  $k$ -space can be more efficiently reconstructed with a fully-sampled reference MRI modality. However, we find that the performance of the aforementioned multi-modal reconstruction can be negatively affected by subtle spatial misalignment between different modalities, which is actually common in clinical practice. In this paper, we improve the quality of multi-modal reconstruction by compensating for such spatial misalignment with a spatial alignment network. First, our spatial alignment network estimates the displacement between the fully-sampled reference and the under-sampled target images, and warps the reference image accordingly. Then, the aligned fully-sampled reference image joins the multi-modal reconstruction of the under-sampled target image. Also, considering the contrast difference between the target and reference images, we have designed a cross-modality-synthesis-based registration loss in combination with the reconstruction loss, to jointly train the spatial alignment network and the reconstruction network. The experiments on both clinical MRI and multi-coil  $k$ -space raw data demonstrate the superiority and robustness of the multi-modal MRI reconstruction empowered with our spatial alignment network. Our code is publicly available at <https://github.com/woxuankai/SpatialAlignmentNetwork>.

**Index Terms**—Image Synthesis, Magnetic Resonance Imaging, MRI Reconstruction, Multi-Modal Reconstruction, Multi-Modal Registration

## I. INTRODUCTION

Magnetic resonance imaging (MRI) is a non-invasive and radiation-free diagnostic technology that has been widely used in clinical practice. However, limited by the device and imaging protocols, MR scan is relatively slow, and the acceleration of MRI acquisition has been an important and everlasting

research topic since its invention. A feasible remedy is to exploit the redundancy between signals received from different coils in parallel imaging [1], [2]. Also, compressed sensing MRI (CS-MRI) [3] allows for accurate reconstruction from the signals that are highly sparse in the  $k$ -space with respect to the Nyquist-Shannon sampling criterion.

Aside from accelerating MRI acquisition by exploiting the intrinsic redundancy within a single MR image, the common information coupled and shared by different MRI sequences draws a lot of attention. In clinical practice, MR images of different contrasts are usually acquired in the same study to reflect different properties of the same region of interest (ROI) and to facilitate precise diagnosis. Recent research [4], [5] has shown that multi-modal MRI reconstruction is better at reconstructing an under-sampled MR sequence (i.e., the *target modality*) with auxiliary information from another fully-sampled *reference modality* in the same study. With the target acquisition under-sampled in the  $k$ -space, the overall time cost of the whole study in MR scanning can thus be reduced.

However, we find that the spatial misalignment between modalities, which is subtle and previously ignored, can non-negligibly weaken the final reconstruction quality of the target modality. Such spatial misalignment is prevalent between individual sequences of the same study. A real example can be found in Fig. 1(a), where the consecutively acquired T1-weighted and T2-weighted images from the same subject are shown. One may easily notice the misalignment of the corresponding anatomic structures as highlighted by the arrows.

The reason behind such misalignment can be complex. Although the subjects are typically instructed to keep still during MRI acquisition, a person even without any MRI knowledge can easily notice the gap between two sequences, e.g., due to pause and altered noises of the scanner. Thus, one may then tend to relax and have subtle movement, which can lead to inconspicuous yet mostly inevitable motion between the sequences, even though external stabilization measures are usually deployed.

However, the spatial misalignment between MRI modalities of the same study is mostly ignored in the literature. With CS-MRI, Lai *et al.* [6] utilized multi-modal image registration to align the reference modality with the intermediate reconstruction result of the under-sampled target modality, while the conventional image registration may not be suitable for the under-sampled MRI. In the recent deep learning era, many reported experiments of multi-modal MRI reconstruction are conducted on carefully registered multi-contrast MRI [7]–[10]. Although image pre-processing can effectively suppress the misalignment for training and validation in labs, such issues

Kai Xuan, Lei Xiang, and Lichi Zhang are with the School of Biomedical Engineering, Shanghai Jiao Tong University, Shanghai, China. (e-mail: {kaixuan, xianglei\_15, lichizhang}@sjtu.edu.cn)

Xiaoqian Huang and Shu Liao are with Shanghai United Imaging Intelligence Co., Ltd., Shanghai, China. (e-mail: {xiaoqian.huang, shu.liao}@united-imaging.com)

Dinggang Shen is with the School of Biomedical Engineering, ShanghaiTech University, Shanghai, China. He is also with Shanghai United Imaging Intelligence Co., Ltd., Shanghai, China. (e-mail: dinggang.shen@gmail.com)

Qian Wang is with the School of Biomedical Engineering, ShanghaiTech University, Shanghai, China. (e-mail: wangqian2@shanghaitech.edu.cn)

This research was supported by the grants from the National Key R&D Program of China (2018YFC0116400), National Natural Science Foundation of China (62131015), Science and Technology Commission of Shanghai Municipality (19QC1400600 and 21010502600), and the Key R&D Program of Guangdong Province, China (2021B0101420006).

can hardly be avoided in real scenarios.

Enlarging model capacity with a deeper neural network is a universal solution towards better performance, but it lacks insight into the spatial misalignment issue and suffers from diminishing marginal utility in multi-modal reconstruction [11]. Alternatively, in this work, we propose an effective solution to explicitly mitigate the negative impact of the spatial misalignment. Particularly, we use a plug-in spatial alignment network to align the reference MRI with the zero-filled target image, in combination with the multi-modal MRI reconstruction network. An overview of our proposed method is shown in Fig. 1(b). First, the spatial alignment network estimates the motion between the fully-sampled reference MRI and the under-sampled target. Then, the warped reference image, instead of the misaligned original one, is concatenated with the under-sampled target and fed into the reconstruction network, which is then able to yield the estimated high-quality target image.

Our contributions are summarized as follows:

- To improve multi-modal MRI reconstruction, we propose to use the spatial alignment network that explicitly compensates for the subtle spatial misalignment between the reference and the target modalities.
- To optimize the spatial alignment network, we propose to combine the cross-modality-synthesis-based loss with the image reconstruction loss, which leads to improved registration and reconstruction quality.
- To demonstrate the superiority and robustness of the proposed method, we propose to conduct extensive experiments on both real-valued clinical MRI and complex-valued multi-coil data.

## II. RELATED WORKS

In this section, we introduce the development of MRI reconstruction in Section II-A firstly, and then the idea of improving target image reconstruction quality with auxiliary information from the reference image in Section II-B. Finally, we discuss multi-modal medical image alignment in Section II-C.

### A. MRI Reconstruction

To recover fully-sampled MR images from partially acquired  $k$ -space signals, image reconstruction plays a key role especially concerning the final image quality. Basic solutions including linear filtering or zero-filling are used to recover the missing  $k$ -space signals, while those relatively simple methods tend to bring in artifacts in the reconstructed MR images. Compressed sensing (CS) [12] and its application to MRI [3] are the milestone of under-sampled MRI reconstruction. The technique has effectively accelerated MRI acquisition.

Deep-learning-based methods emerge as state-of-the-art in MRI reconstruction. In the pilot work of Wang *et al.* [13], a convolutional neural network (CNN) is trained offline to model the mapping from zero-filled under-sampled MR images to the corresponding fully-sampled ones. Later, the techniques such as data consistency layers [14] and recurrent neural networks (RNNs) [15] are used to further improve the reconstruction quality. While most works follow the image-space modeling

paradigm used in CS-MRI, Han *et al.* [16] proposed to estimate the missing MR signals in the  $k$ -space where MRI is physically acquired. Further, Zhang *et al.* [17] processed MRI signals in both image space and  $k$ -space. Another interesting deep-learning-based solution for MRI reconstruction is to directly estimate the fully-sampled MR images from partially acquired  $k$ -space signals without invoking Fourier transform explicitly [18]. Recently, the NYU fastMRI challenges, especially the large-scale public datasets, have greatly promoted the development of reconstruction algorithms [19]–[22].

While the works mentioned above focus on the reconstruction of a single MRI modality independently, our proposed method takes multiple MRI modalities into consideration during the multi-modal reconstruction.

### B. Reference-based MRI Reconstruction

With physiology-related redundancy between MR images, reconstructing under-sampled MRI with auxiliary information from reference images is promising. Regarding multiple visits of the same patient, Souza *et al.* [23] proposed to accelerate MRI follow-ups with early intra-subject images. Weizman *et al.* [24], [25] proposed a more flexible solution for the case when the reference was not fully available. Schlemper *et al.* [14] took advantage of the redundancy between adjacent temporal frames of dynamic MRI by learning the temporal correlation with 3D convolution (2D + time). Moreover, the redundancy between spatially neighboring 2D slices in a 3D volume was used in Hirabayashi *et al.* [26], to improve the reconstruction quality by fully-sampling selected slices while under-sampling the rest.

The reconstruction of a certain MRI modality can be enhanced with the help from other modalities, as a typical MRI study consists of multiple sequences and they are usually acquired sequentially. Majumdar *et al.* [27] and Huang *et al.* [28] jointly reconstructed T1- and T2-weighted images of the same ROI from under-sampled MRI signals. For learning-based methods, Song *et al.* [29] proposed coupled dictionary learning for multi-contrast MRI reconstruction. More recently, with deep neural networks, Kim *et al.* [5] and Xiang *et al.* [4] proposed to speed up T2-weighted acquisition by integrating T1-weighted image as the reference into the reconstruction process. More techniques, such as progressive neural networks [9], generative adversarial networks [10], and dilated convolutions [8], are also investigated to improve multi-modal MRI reconstruction. Also, note that multi-modal reconstruction is not only limited to MRI. The idea has been successfully used in various tasks, e.g., enhancing low-dose positron emission tomography (PET) quality with corresponding MRI to reduce the radiation risk of PET/MRI scanning [30].

Different from merging information from varying references, our proposed method focuses on mitigating the spatial misalignment between the target and reference images, which is mostly ignored by literature reports but can hardly be avoided in real scenarios.

### C. Multi-Modal MRI Alignment

Image registration is a classical topic in medical image analysis, and it is developing fast nowadays when enabled

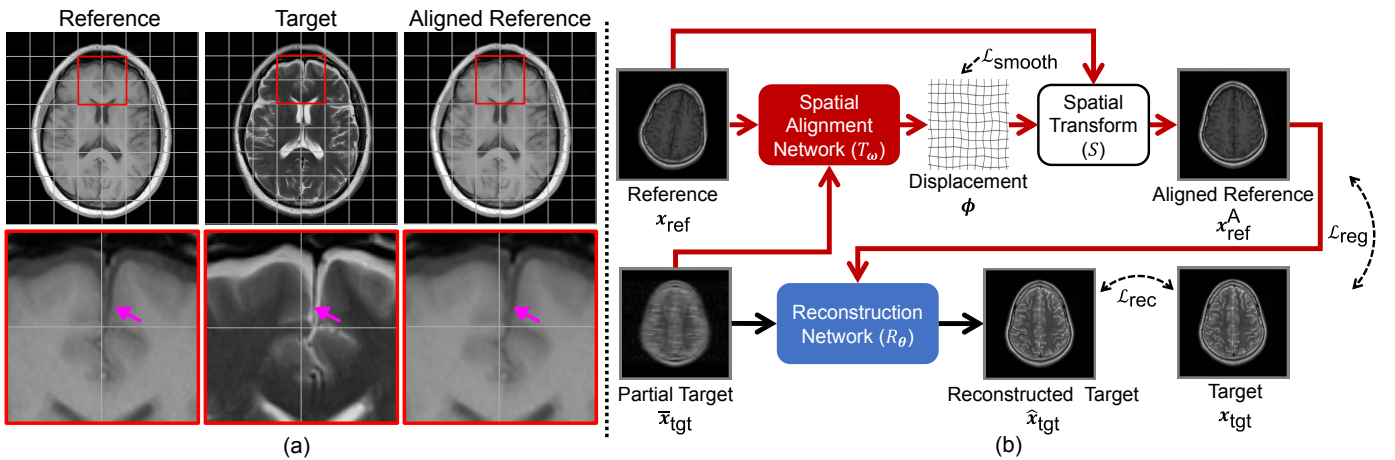


Fig. 1. A real case demonstrating the existence of spatial misalignment (a), and the overview of the proposed method (b). In (a), a real case of multi-modal MRI acquired for the diagnostic purpose demonstrates the existence of spatial misalignment (highlighted by arrows) between the reference (T1-weighted) and the target (T2-weighted) images. The aligned reference image is also available to show the effect of our proposed spatial alignment network. In (b), a spatial alignment network is integrated into the multi-modal MRI reconstruction pipeline to compensate for the spatial misalignment between the fully-sampled reference image and the under-sampled target. The data flow for the conventional deep-learning-based reconstruction is shown in black arrows, and the red arrows are for additional data flow related to our proposed spatial alignment network.

with deep learning. Traditional methods take registration as an optimization problem, and the displacement field is optimized iteratively with an objective function consisting of the image similarity loss and the regularization term. Such methods are popular, including ANTs [31], Demons [32], [33], and SPM [34]. In the alternative, learning-based methods, especially for deep-learning-based registration, the complex displacement field can be directly learned between the fixed and the moving images. Early works train deep neural networks to predict the displacement fields in a supervised manner [35]. And later, Balakrishnan *et al.* [36] proposed to train registration networks in an unsupervised manner. While image registration methods usually focus on fully-sampled images, Kustner *et al.* [37] showed the feasibility to directly register under-sampled MR images. They also explored the way to estimate the displacement fields in Fourier space instead of image space.

It is critical to design accurate and robust metrics to quantify image similarity, especially in the case of multi-modal or multi-contrast registration. However, such metrics are challenging to design in computer vision due to the huge appearance gap across different image modalities. Mutual information (MI), describing the pixel- or voxel-wise statistical dependency between corresponding intensities of the images to be aligned [38], has been successfully applied to various multi-modal image registration tasks, e.g., PET-computed tomography (CT) [39], and PET-MRI registration [40]. Later, feature-based similarity metrics such as modality independent neighborhood descriptor (MIND) [41] take use of high-order appearance features to establish spatial correspondences. With deep learning, Fan *et al.* [42] proposed to measure the image similarity with the generative adversarial network (GAN), but paired images were required in their work as training samples. Cao *et al.* [43] circumvented the direct similarity measurement with cross-modality synthesis. They thus could replace the difficult calculation of multi-modal similarity with

a much simpler mono-modal metric. Further, to prevent possible spatial distortion introduced by cross-modality synthesis, the geometric-preserving technique was adopted in Arar *et al.* [44].

Similar to Arar *et al.* [44], our proposed method attains geometric-preserving cross-modality-synthesis-based registration through the spatial alignment network. Note that our registration handles under-sampled MR images, while existing registration methods usually focus on fully-sampled MRI.

### III. METHODS

The framework of our proposed method is illustrated in Fig. 1(b). It includes (1) the spatial alignment network to register the reference image with the under-sampled target, and (2) the reconstruction network to restore the target modality image of high quality. Three major loss functions play critical roles in our framework. Other than the commonly used smoothness constraint  $\mathcal{L}_{\text{smooth}}$  upon the displacement field, we also calculate the reconstruction loss  $\mathcal{L}_{\text{rec}}$  and the registration loss  $\mathcal{L}_{\text{reg}}$  to train the spatial alignment network and the reconstruction network jointly.

The rest of Section III will be arranged as follows. Section III-A presents the mathematical formulation of multi-modal MRI reconstruction aided by the spatial alignment network. Then, the three loss functions, i.e., the smoothness constraint  $\mathcal{L}_{\text{smooth}}$ , the reconstruction loss  $\mathcal{L}_{\text{rec}}$  and the registration loss  $\mathcal{L}_{\text{reg}}$ , are described in Section III-B. Finally, in Section III-C, we introduce more implementation details.

#### A. Multi-Modal MRI Reconstruction

In this subsection, we first formulate the learning-based MRI reconstruction, and then introduce the multi-modal MRI reconstruction. Next, we discuss how to integrate the proposed spatial alignment network into the multi-modal MRI reconstruction pipeline.



1) *MRI Reconstruction*: The MRI acquisition can be perceived as sampling in a full  $k$ -space. Taking 2D MRI of the image shape of  $N_x \times N_y$  for example, with a flattened complex-valued fully-sampled MRI image  $\mathbf{x} \in \mathbb{C}^N$  where  $N = N_x \times N_y$ , the fast MRI acquisition process can be expressed as  $\mathbf{y} = \mathbf{F}_u \mathbf{x}$ , where  $\mathbf{y} \in \mathbb{C}^M$  is the under-sampled MR signals in the  $k$ -space with the sampling ratio  $\frac{M}{N}$ , ( $M \leq N$ ).  $\mathbf{F}_u \in \mathbb{C}^{M \times N}$ , being consistent with notations in Lustig *et al.* [3], is a matrix representing the whole MRI under-sampling process which usually consists of the Fourier transform and the  $k$ -space under-sampling. Note that the number of coils is ignored here for simplicity, though the above formulation can be easily extended to the multi-coil setting.

Without loss of generality, the deep-learning-based MRI reconstruction, which estimates the fully-sampled MRI  $\mathbf{x}$  from the under-sampled  $k$ -space signals  $\mathbf{y}$ , can be denoted as  $R_\theta$ . Here, for a modern MRI reconstruction method like the End-to-End Variational Networks (E2E-VarNet) [45],  $R_\theta$  usually contains a serial of neural network blocks and data consistency layers [14], and  $\theta$  is the union set of all learnable parameters. Before feeding to  $R_\theta$ , usually the raw acquisition  $\mathbf{y}$  is pre-processed with  $\mathbf{F}_{0\text{-fill}}^{-1} \in \mathbb{C}^{N \times M}$ , which represents zero-filling of the missing MR signals and inverse Fourier transform mapping the  $k$ -space data back to the image space. In this way, one can have the under-sampled MR image  $\bar{\mathbf{x}} = \mathbf{F}_{0\text{-fill}}^{-1} \mathbf{y}$ , where  $\bar{\mathbf{x}} \in \mathbb{C}^N$ . Next, as aliasing ghosts typically exist in  $\bar{\mathbf{x}}$ , the reconstruction model  $R_\theta$  should be capable of restoring the fully-sampled MRI from the under-sampled one, i.e.,  $\hat{\mathbf{x}} = R_\theta(\bar{\mathbf{x}})$ . As a result,  $R_\theta$  is often referred as the de-aliasing model.

2) *Multi-Modal MRI Reconstruction*: The target MR image  $\mathbf{x}_{\text{tgt}}$  can be better reconstructed with the help of the reference, such as an image of the same ROI yet of different contrast acquired in the same study. Extracting common information from the reference image of a different contrast is non-trivial. And in the context of deep learning, this process is expected to be completed in a sophisticated data-driven and encoding-decoding way.

In early works [4], [5], the fully-sampled reference modality  $\mathbf{x}_{\text{ref}}^A$  and the under-sampled target modality  $\bar{\mathbf{x}}_{\text{tgt}}$  are concatenated in the channel dimension, and fed into a single reconstruction model  $R_\theta$ . It is expected that  $\mathbf{x}_{\text{ref}}^A$  can help reconstruct  $\mathbf{x}_{\text{tgt}}$ , as the network should fuse individual channels of inputs and feature maps through forward convolution. As a summary, the multi-modal MRI reconstruction process can be formulated as  $\hat{\mathbf{x}}_{\text{tgt}} = R_\theta(\bar{\mathbf{x}}_{\text{tgt}}, \mathbf{x}_{\text{ref}}^A)$ . The superscript A of  $\mathbf{x}_{\text{ref}}^A$  indicates that the reference image is well-aligned to the target modality virtually.

3) *Spatial Alignment Network*: In this work, we propose to integrate a spatial alignment network  $T_\omega$  into the multi-modal MRI reconstruction, in order to estimate and compensate for the subtle spatial misalignment between the target and the reference modalities. First, the spatial alignment network explicitly estimates the displacement field  $\phi$  between the under-sampled target modality  $\bar{\mathbf{x}}_{\text{tgt}}$  and the fully-sampled reference modality  $\mathbf{x}_{\text{ref}}$  following

$$\phi = T_\omega(\bar{\mathbf{x}}_{\text{tgt}}, \mathbf{x}_{\text{ref}}), \quad (1)$$

where  $\phi \in \mathbb{R}^{2 \times N}$  in our implementation. Then, a spatial transformation layer  $S$  is employed to warp the fully-sampled reference  $\mathbf{x}_{\text{ref}}$  according to the estimated displacement field  $\phi$ . Specifically, in the position  $\mathbf{p}$ ,  $S(\phi, \mathbf{x}_{\text{ref}})[\mathbf{p}] = \mathbf{x}_{\text{ref}}[\mathbf{p} + \phi[\mathbf{p}]]$ . Finally, the spatially aligned image of the fully-sampled reference  $\mathbf{x}_{\text{ref}}^A = S(\phi, \mathbf{x}_{\text{ref}})$  is fed into the multi-modal reconstruction network together with the under-sampled target modality  $\bar{\mathbf{x}}_{\text{tgt}}$ , and the whole multi-modal MRI reconstruction process becomes

$$\hat{\mathbf{x}}_{\text{tgt}} = R_\theta(\bar{\mathbf{x}}_{\text{tgt}}, S(\phi, \mathbf{x}_{\text{ref}})). \quad (2)$$

Also, note that usually both fully-sampled reference and target images are required to estimate their spatial misalignment. However, in our setting, the fully-sampled target image is not available before reconstruction, thus  $T_\omega$  takes an input of the under-sampled target modality (after zero-filling) instead of the fully-sampled one.

## B. Loss Designs

To optimize the spatial alignment network as well as the multi-modal MRI reconstruction network, three loss functions are used in this work. First, the smoothness loss  $\mathcal{L}_{\text{smooth}}$  is imposed in favor of a physically reasonable displacement field. Then, the reconstruction loss  $\mathcal{L}_{\text{rec}}$  asks for high fidelity of the reconstruction result, which also implicitly encourages accurate spatial alignment between the target and the reference. Finally, the registration loss  $\mathcal{L}_{\text{reg}}$  is proposed to provide explicit guidance to optimize the spatial alignment network and to contribute to high reconstruction quality.

1) *Smoothness Loss*: It is common to impose smooth prior on the estimated displacement field  $\phi$  in image registration. In our implementation, the smoothness loss is defined as  $\mathcal{L}_{\text{smooth}} = \frac{1}{N} \|\nabla \phi\|_2^2$ . For 2D MRI,  $\mathcal{L}_{\text{smooth}}$  is expanded as

$$\mathcal{L}_{\text{smooth}} = \frac{1}{N} \sum_{\mathbf{p}} \left( \frac{\partial \phi_x}{\partial x} [\mathbf{p}] \right)^2 + \left( \frac{\partial \phi_x}{\partial y} [\mathbf{p}] \right)^2 + \left( \frac{\partial \phi_y}{\partial x} [\mathbf{p}] \right)^2 + \left( \frac{\partial \phi_y}{\partial y} [\mathbf{p}] \right)^2. \quad (3)$$

2) *Reconstruction Loss*: The image reconstruction loss  $\mathcal{L}_{\text{rec}}$  is required to guide the optimization of the reconstruction network  $R_\theta$ . It is also possible to optimize the spatial alignment network  $T_\omega$  with the hint from the reconstruction loss, as the high-quality reconstruction of the target usually desires accurate spatial alignment between the two images.

In Fig. 1(b), the reconstruction loss  $\mathcal{L}_{\text{rec}}$  is applied to the output of the reconstruction network, and its gradient updates both the reconstruction network  $R_\theta$  and the spatial alignment network  $T_\omega$  though back-propagation. In particular, we use the popular structural similarity (SSIM) [45], [46] as the reconstruction loss, i.e.,

$$\mathcal{L}_{\text{rec}} = -\text{SSIM}(\hat{\mathbf{x}}_{\text{tgt}}, \mathbf{x}_{\text{tgt}}). \quad (4)$$

3) *Registration Loss*: Using only the reconstruction loss may not be sufficient to optimize the spatial alignment network, as the back-propagation pathway is too long for the reconstruction loss  $\mathcal{L}_{\text{rec}}$  to reach the spatial alignment network.

As the result, we propose to optimize the spatial alignment network with the direct multi-modal MRI registration loss  $\mathcal{L}_{\text{reg}}$ , which aims to maximize the similarity between the target and the aligned reference images.

It is challenging though to design the image similarity metric especially for multi-modal image registration. Recently, cross-modality image synthesis has provided a new feasible solution to this problem [43]. Instead of directly measuring the similarity between the target  $\mathbf{x}_{\text{tgt}}$  and the aligned reference  $\mathbf{x}_{\text{ref}}^{\text{A}}$ , we first use a cross-modal synthesis network  $G_{\rho}$  (marked with green boxes in Fig. 2) to produce the synthesized target image  $\mathbf{x}_{\text{ref}}^{\text{S}} = G_{\rho}(\mathbf{x}_{\text{ref}})$ . Then, the registration tends to align  $\mathbf{x}_{\text{ref}}^{\text{S}}$  (instead of  $\mathbf{x}_{\text{ref}}$ ) and produces  $\mathbf{x}_{\text{ref}}^{\text{SA}} = S(\phi, \mathbf{x}_{\text{ref}}^{\text{S}})$ . Next, we can easily calculate  $\mathcal{L}_{\text{reg}}^{\text{SA}} = \|\mathbf{x}_{\text{tgt}} - \mathbf{x}_{\text{ref}}^{\text{SA}}\|_1$  and treat it as the dissimilarity between  $\mathbf{x}_{\text{tgt}}$  and  $\mathbf{x}_{\text{ref}}^{\text{SA}}$ . Note that the superscript SA indicates the ‘‘synthesis-align (SA)’’ strategy.

The cross-modality synthesis network  $G_{\rho}$  needs to be geometry-preserving. That is, before/after synthesis, the same anatomical structures in the input/output images of  $G_{\rho}$  should be spatially aligned, even though the images are of different modalities in appearance. To this end, we follow Arar *et al.* [44] and use the dual-path registration scheme as in Fig. 2. Specifically, in addition to the previous introduced loss  $\mathcal{L}_{\text{reg}}^{\text{SA}}$ , we can place the cross-modality synthesis network after the spatial transform layer. In this way, we can derive the ‘‘align-synthesis (AS)’’ branch (in the top of Fig. 2), which is different from the SA branch at the bottom of the figure. Note that the two branches share the same cross-modality synthesis network parameters. In this way, the final registration loss is a mixture of SA and AS:

$$\mathcal{L}_{\text{reg}} = 0.5 \underbrace{\|\mathbf{x}_{\text{tgt}} - \mathbf{x}_{\text{ref}}^{\text{SA}}\|_1}_{\text{SA}} + 0.5 \underbrace{\|\mathbf{x}_{\text{tgt}} - \mathbf{x}_{\text{ref}}^{\text{AS}}\|_1}_{\text{AS}}. \quad (5)$$

The above  $\mathcal{L}_{\text{reg}}$  also implicitly promotes  $\mathbf{x}_{\text{ref}}^{\text{SA}} = \mathbf{x}_{\text{ref}}^{\text{AS}}$ .

### C. Implementation Details

In this subsection, we introduce more details of our implementation, including the adversarial optimization of the cross-modality synthesis network, and the full algorithm of our multi-modal MRI reconstruction integrated with the spatial alignment network.

1) *Adversarial Loss*: To optimize the cross-modality synthesis network  $G_{\rho}$ , other than the registration loss  $\mathcal{L}_{\text{reg}}$ , the adversarial loss  $\mathcal{L}_{\text{adv}}$  is additionally used to encourage more realistic synthesized images. While the registration loss  $\mathcal{L}_{\text{reg}}$  measures the mean absolute error between the synthesized and the real target images, the adversarial loss involves a discriminator  $D_{\gamma}$  that forces the synthesized images to be less distinguishable from the real ones. Following the adversarial training, the generator  $G_{\rho}$  and the discriminator  $D_{\gamma}$  are optimized alternatively. More specifically, spectral normalization [47] and hinge loss are used. Also, the adversarial loss considers both SA and AS branches as shown in Fig. 2:

$$\mathcal{L}_{\text{adv}} = D_{\gamma}(\mathbf{x}_{\text{tgt}}) - 0.5D_{\gamma}(\mathbf{x}_{\text{ref}}^{\text{SA}}) - 0.5D_{\gamma}(\mathbf{x}_{\text{ref}}^{\text{AS}}). \quad (6)$$

The optimization of the cross-modality synthesis network  $G_{\rho}$  and discriminator  $D_{\gamma}$  can thus be formulated as

$$\rho^*, \gamma^* = \arg \min_{\rho} \max_{\gamma} \mathbb{E}_{p((\mathbf{x}_{\text{tgt}}, \mathbf{x}_{\text{ref}}))} \alpha \mathcal{L}_{\text{reg}} + \beta \mathcal{L}_{\text{adv}}. \quad (7)$$

2) *Hybrid Supervision over Spatial Alignment Network*: To take advantage of both reconstruction and registration losses towards better spatial aligning and reconstruction quality, hybrid supervision is imposed on the spatial alignment network. The optimizing of the spatial alignment network solely with the reconstruction loss may be limited due to the long back-propagation pathway, while the direct supervision from only the registration loss network may deviate from the final goal of high-quality image reconstruction. Thus, with both two loss functions, we combine them as the hybrid supervision upon the spatial alignment network  $T_{\omega}$  and the multi-modal reconstruction network  $R_{\theta}$ :

$$\theta^*, \omega^* = \arg \min_{\theta, \omega} \mathbb{E}_{p((\mathbf{x}_{\text{tgt}}, \mathbf{x}_{\text{ref}}))} \mathcal{L}_{\text{rec}} + \lambda \mathcal{L}_{\text{smooth}} + \alpha \mathcal{L}_{\text{reg}}. \quad (8)$$

The full training scheme of the multi-modal reconstruction with the spatial alignment network optimized with hybrid reconstruction and registration losses is summarized as follows.

**Data**: Fully-sampled multi-modal MR images from same studies,  $\{(\mathbf{x}_{\text{tgt}}, \mathbf{x}_{\text{ref}})\}$ .

**Output**: Optimized neural networks,  $R_{\theta^*}$ ,  $T_{\omega^*}$ ,  $G_{\rho^*}$ , and  $D_{\gamma^*}$ .

#### 1: repeat

2:  $\mathbf{x}_{\text{tgt}}, \mathbf{x}_{\text{ref}} \leftarrow p((\mathbf{x}_{\text{tgt}}, \mathbf{x}_{\text{ref}}))$

3:  $\tilde{\mathbf{x}}_{\text{tgt}} \leftarrow \mathbf{F}_{0\text{-fill}}^{-1} \mathbf{F}_u \mathbf{x}_{\text{tgt}}$

4:  $\phi \leftarrow T_{\omega}(\tilde{\mathbf{x}}_{\text{tgt}}, \mathbf{x}_{\text{ref}})$

5:  $\hat{\mathbf{x}}_{\text{tgt}} \leftarrow R_{\theta}(\tilde{\mathbf{x}}_{\text{tgt}}, S(\phi, \mathbf{x}_{\text{ref}}))$

6:  $\mathbf{x}_{\text{ref}}^{\text{SA}}, \mathbf{x}_{\text{ref}}^{\text{AS}} \leftarrow S(\phi, G_{\rho}(\mathbf{x}_{\text{ref}})), G_{\rho}(S(\phi, \mathbf{x}_{\text{ref}}))$

7: Calculate  $\mathcal{L}_{\text{smooth}}$ ,  $\mathcal{L}_{\text{rec}}$ ,  $\mathcal{L}_{\text{reg}}$ , and  $\mathcal{L}_{\text{adv}}$  with (3), (4), (5), and (6), separately.

8:  $\theta \leftarrow \theta - \eta \partial_{\theta} \mathcal{L}_{\text{rec}}$

9:  $\omega \leftarrow \omega - \eta \partial_{\omega} (\mathcal{L}_{\text{rec}} + \lambda \mathcal{L}_{\text{smooth}} + \alpha \mathcal{L}_{\text{reg}})$

10:  $\rho \leftarrow \rho - \eta \partial_{\rho} (\alpha \mathcal{L}_{\text{reg}} + \beta \mathcal{L}_{\text{adv}})$

11:  $\gamma \leftarrow \gamma + \eta \partial_{\gamma} (\beta \mathcal{L}_{\text{adv}})$

12: **until** convergence

where  $\lambda$ ,  $\alpha$ , and  $\beta$  are the weights for  $\mathcal{L}_{\text{smooth}}$ ,  $\mathcal{L}_{\text{reg}}$ , and  $\mathcal{L}_{\text{adv}}$ , and  $\eta$  is the learning rate.

Hyper-parameters are selected on the validation set of section IV-A. In our implementation, a large weight ( $\lambda = 1000$ ) is used for the smoothness loss  $\mathcal{L}_{\text{smooth}}$  of intra-subject registration. The weight for the synthesis-based image registration loss  $\mathcal{L}_{\text{reg}}$  providing direct guidance to the optimization process is set to 0.1 (i.e.  $\alpha = 0.1$ ), as experiments demonstrate that a smaller  $\alpha$  is insufficient to align multi-modal MRI, while a larger  $\alpha$  is also harmful because  $\mathcal{L}_{\text{reg}}$  is not exactly consistent with the goal of MRI reconstruction. Moreover, the weight for our adversarial loss  $\mathcal{L}_{\text{adv}}$  is set to 0.01 (i.e.  $\beta = 0.01$ ), and a smaller  $\beta$  may lead to unstable adversarial training.

## IV. EXPERIMENTS

The experiments are conducted on two MRI datasets. The first dataset contains real-valued single-coil MRI stored in

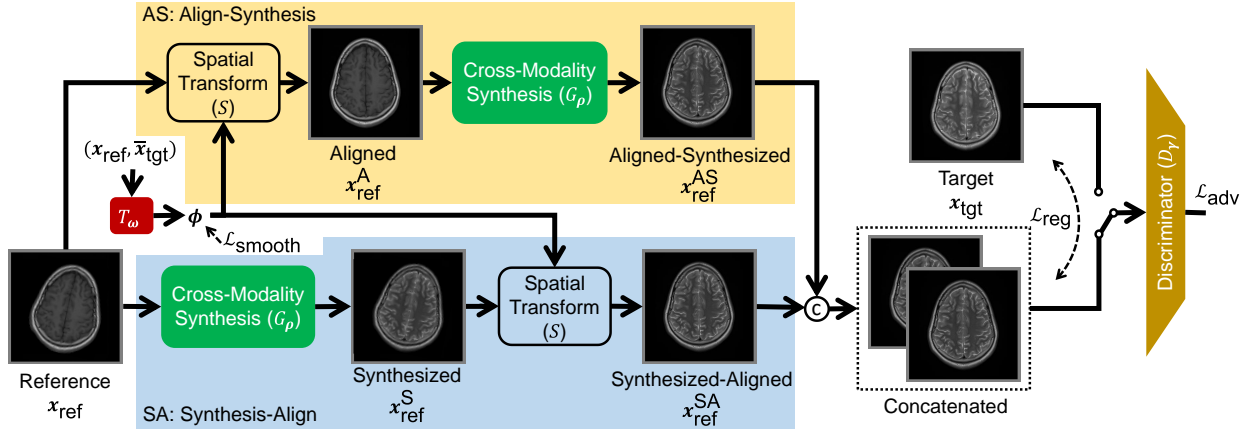


Fig. 2. Illustration of the registration loss  $\mathcal{L}_{reg}$ . To measure the cross-modal image similarity between the aligned reference image and the target modality, a cross-modality synthesis network is employed to generate the corresponding target modality from the reference modality. Then we use mono-modality similarity to quantify the difference between the synthesized and real target images. We can either place the synthesis network  $G_\rho$  after and before the spatial transform layer  $S$ , which derives the align-synthesis (AS) and synthesis-align (SA) branches, respectively. Finally, a discriminator is employed in favor of realistic synthesized images.

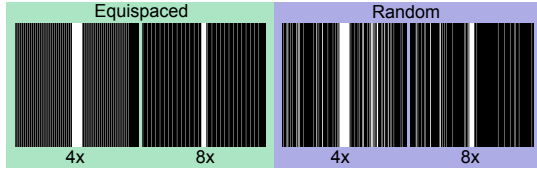


Fig. 3. The  $k$ -space under-sampling patterns. Numbers at the bottom of individual patterns indicate the acceleration factors.

digital imaging and communications in medicine (DICOM) format collected from the large and publicly accessible NYU fastMRI Initiative database<sup>1</sup> [19], [20] (“DICOM dataset”, Section IV-A), and the second one consists of in-house complex-valued multi-coil raw MR images (“raw dataset”, Section IV-B). Finally, ablation studies are provided in Section IV-C.

In both experiments, following the paradigm of fastMRI challenge, the under-sampled MRI is acquired by down-sampling corresponding fully-sampled MRI in the  $k$ -space with a predefined Cartesian sampling pattern. More specifically, two typical sampling patterns — the random and equispaced sampling patterns — are used in our experiments, with a sampling ratio of 25% or 12.5%, respectively. Considering the low-frequency signals contain most of the energy in the  $k$ -space, for both random and equispaced patterns, 32% of the sampling is always allocated to the low frequency, while the rest sampling is distributed randomly or equispaced. The under-sampling patterns used in the experiments are shown in Fig. 3.

The E2E-VarNet [45], with minimal modification to work with multi-modal MRI, is employed as the backbone of the reconstruction network. The U-Net [48] variant similar to that in Balakrishnan *et al.* [36] is used as our spatial alignment network. Similar to Isola *et al.* [49], our generator is the U-Net [48] empowered with batch normalization [50], and our discriminator is a stack of normalization-

activation-convolution paradigms. Considering all MR images are scanned with large slice spacing and thickness, 2D slices are extracted from 3D volumes for training and evaluation.

Our implementation is mainly based on PyTorch library [51] and the neural networks are trained on Nvidia TITAN RTX graphics cards. The Adam optimizer [52] with the learning rate of  $\eta = 0.0001$  and batch size of 4 is used in all experiments. Also, the early-stop strategy of 20,000 iterations, which take about 3 hours with our hybrid optimization, is used to prevent over-fitting. Finally, with the best checkpoint selected on the validation set, performances on an independent test set are measured and reported. More implementation details can be found in our supplementary materials and released code.

#### A. Experiments on DICOM Dataset

We first run our proposed method on the real-valued single-coil MR images recompiled from the fastMRI database. While multi-modal MRI is not explicitly provided by fastMRI, we iterate over all DICOM studies and select paired T1- and T2-weighted axial brain MRIs. Finally, 340 pairs of T1- and T2-weighted MR images are extracted. Among them, 170 pairs of volumes (2720 pairs of slices) are used for training, 68 pairs of volumes (1088 pairs of slices) are taken as the validation set, and the rest 102 pairs of volumes (1632 pairs of slices) are for testing. For both T1- and T2-weighted images, the in-plane size is  $320 \times 320$ , the resolution is  $0.68\text{mm} \times 0.68\text{mm}$ , and the slice spacing is 5mm. In our experiments, fully-sampled T1-weighted MRI is used to help the reconstruction of under-sampled T2-weighted image, which is consistent with early literature reports [4], [5]. It is also expected that T2-weighted MRI can help T1-weighted MRI reconstruction, and joint reconstruction of both under-sampled T1- and T2-weighted MR images can achieve high efficiency due to their mutually shared information.

We also find that data augmentation can benefit the reconstruction. More specifically, for each pair of multi-modal MRI and in each epoch, a randomly generated deformation

<sup>1</sup><https://fastmri.med.nyu.edu/>



TABLE I

QUANTITATIVE COMPARISON OF RECONSTRUCTION RESULTS ON DICOM DATASET. IN “MULTI-MODAL” AND “PROPOSED” SETTINGS, THE UNDER-SAMPLED T2-WEIGHTED MRI IS RECONSTRUCTED WITH HELPS OF FULLY-SAMPLED T1-WEIGHTED IMAGE. FOR ALL SETTINGS AND METRICS, “MULTI-MODAL” IS SIGNIFICANTLY BETTER THAN “SINGLE-MODAL”, AND “PROPOSED” IS SIGNIFICANTLY BETTER THAN “MULTI-MODAL” ( $p < 0.01$  WITH PAIRED  $t$ -TESTS).

		4× Acceleration		8× Acceleration	
		PSNR	SSIM	PSNR	SSIM
Equispaced	Single-Modal	38.89 ±1.66	0.9762 ±0.0067	37.01 ±1.77	0.9674 ±0.0091
	Multi-Modal	40.32 ±1.91	0.9809 ±0.0072	38.80 ±2.11	0.9755 ±0.0098
	Proposed	<b>40.81</b> ±1.92	<b>0.9821</b> ±0.0069	<b>39.38</b> ±2.06	<b>0.9775</b> ±0.0088
Random	Single-Modal	42.72 ±1.81	0.9867 ±0.0043	35.50 ±1.73	0.9600 ±0.0103
	Multi-Modal	43.57 ±1.95	0.9882 ±0.0046	37.42 ±2.00	0.9705 ±0.0109
	Proposed	<b>43.91</b> ±1.94	<b>0.9888</b> ±0.0043	<b>38.06</b> ±2.04	<b>0.9729</b> ±0.0103

field is applied to both fully-sampled target and reference images. The deformation field is a combination of random rotation ( $[-0.01\pi, 0.01\pi]$ ), translation ( $[-0.05N, 0.05N]$ ), and the deformation bicubically interpolated from  $9 \times 9$  control-points (each assigned with a random displacement in the range of  $[-0.02N, 0.02N]$ , where  $N$  is the size of the MR images).

Table I compares the MRI reconstruction performance with different under-sampling settings and reconstruction methods. Particularly, “Single-Modal” is our single-modal baseline, where E2E-VarNet [45] reconstructs T2-weighted MRI without using T1 reference. “Multi-Modal” is the multi-modal baseline, which simply adds T1 reference to E2E-VarNet [45]. The “Proposed” method further integrates the spatial alignment network with multi-modal E2E-VarNet. It is observed that the “Multi-Modal” baseline is significantly ( $p < 0.01$  with paired  $t$ -test) better than “Single-Modal” in both peak signal-to-noise ratio (PSNR, the higher, the better) and SSIM (the higher, the better) in all settings. Compared to “Multi-Modal”, the reconstruction performance can be further improved with our “Proposed” method significantly and consistently.

Further, a visual comparison of the reconstruction quality is provided in Fig. 4. In general, the multi-modal reconstruction produces clearer MRI images compared with the single-modal reconstruction, and our “Proposed” method further brings in more details. For example, the signals in cyan and yellow circles are missing in “Single-Modal” MRI reconstruction. With a reference modality (“Multi-Modal”), such signals are less indistinguishable but still vague. Finally, when the spatial alignment network is integrated, one can observe a dark vertical line in the cyan circle and dark scratch-like signals in the yellow circle. Another example is pointed by the magenta arrows, where the reconstruction constantly gets clearer from “Single-Modal”, “Multi-Modal” to “Proposed”. The error maps, which subtract the reconstructed target images from the ground-truth, are also consistent with the quantitative comparisons in Table I, as the errors decrease after the spatial alignment network is integrated.

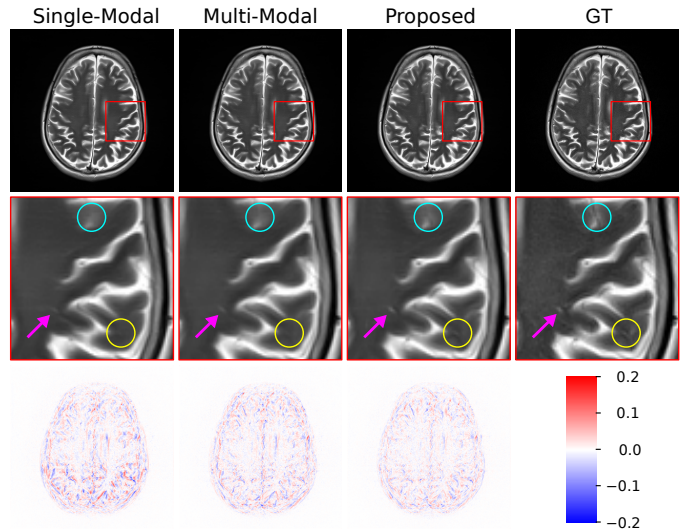


Fig. 4. Visual comparison of the reconstructed target MR images on DICOM dataset. Results of the equispaced under-sampling pattern at  $8\times$  acceleration ratio are compared. The first row is for the reconstructed images, with the red bounding-boxes zoomed-in in the second row. The corresponding error maps are provided in the third row.

### B. Experiments on Multi-Coil Dataset

In this subsection, we conduct experiments on our raw dataset which contains in-house complex-valued 24-channel 3T MR images with raw  $k$ -space data. We collect a total of 62 studies, where each study contains paired T1-weighted fluid-attenuated inversion recovery (T1-FLAIR, TR=2015ms, TE=12ms) and T2-weighted (TR=4226ms, TE=104.8ms) MRI. The in-plane spacing is  $0.7\text{mm} \times 0.7\text{mm}$ , slice thickness is 5mm, and spatial size of each slice is also  $320 \times 320$ . Again, 2D slices are extracted from individual volumes, and T2-weight MR images are supposed to be the target modality. More specifically, 25 subjects (503 pairs of slices) are used for training, 12 subjects (241 pairs of slices) are for validation, and the rest 25 subjects (504 pairs of slices) are for testing. Again, data augmentation is used considering the limited number of training data.

Quantitative comparison of different reconstruction methods can be found in Table II. Compared to the popular “Single-Modal” reconstruction, the information from the reference modality (“Multi-Modal”) can significantly improve the reconstruction performance in all settings and metrics. Also, with our spatial alignment network integrated to multi-modal reconstruction (“Proposed”), the metrics of the final reconstruction quality are further significantly improved.

Fig. 5 visually illustrates the reconstruction results and corresponding error maps of T2-weighted MRI under-sampled with the random sampling pattern at  $8\times$  acceleration ratio. Generally speaking, visual quality and error maps monotonically get better from “Single-Modal”, “Multi-Modal” to “Proposed”, which is consistent with Table II. More specifically, comparing “Multi-Modal” and “Single-Modal”, the tissue boundaries are sharper in MR images reconstructed with the reference modality, including but not limited to the white matter (WM) / gray matter (GM) boundary pointed by magenta arrows. Comparing “Proposed” and “Multi-Modal”,

TABLE II  
 QUANTITATIVE COMPARISON OF THE RECONSTRUCTION RESULTS ON PRIVATE MULTI-COIL MRI DATASET WITH REAL  $k$ -SPACE DATA. THE UNDER-SAMPLED T2-WEIGHTED MRI IS RECONSTRUCTED WITH HELPS OF THE FULLY-SAMPLED T1-FLAIR IMAGE. FOR ALL SETTINGS AND METRICS, “MULTI-MODAL” IS SIGNIFICANTLY BETTER THAN “SINGLE-MODAL”, AND “PROPOSED” IS SIGNIFICANTLY BETTER THAN “MULTI-MODAL” ( $p < 0.01$  WITH PAIRED  $t$ -TESTS).

		4× Acceleration		8× Acceleration	
		PSNR	SSIM	PSNR	SSIM
Equispaced	Single-Modal	39.49 ±1.04	0.9603 ±0.0110	35.31 ±0.90	0.9309 ±0.0151
	Multi-Modal	39.60 ±1.23	0.9611 ±0.0114	35.50 ±1.43	0.9356 ±0.0190
	Proposed	<b>40.14</b> ±1.24	<b>0.9637</b> ±0.0110	<b>36.27</b> ±1.43	<b>0.9387</b> ±0.0183
Random	Single-Modal	38.59 ±0.94	0.9577 ±0.0107	33.14 ±0.86	0.9086 ±0.0161
	Multi-Modal	38.90 ±1.31	0.9580 ±0.0119	34.11 ±1.54	0.9240 ±0.0231
	Proposed	<b>39.45</b> ±1.24	<b>0.9603</b> ±0.0111	<b>34.65</b> ±1.52	<b>0.9291</b> ±0.0222

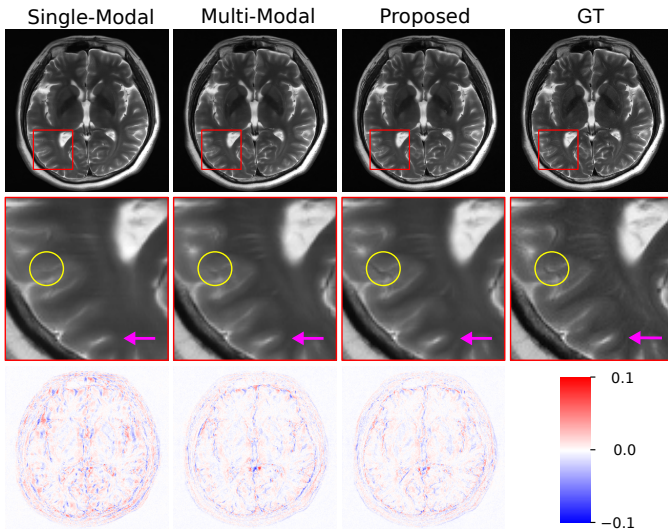


Fig. 5. Visual comparison of the reconstructed images, zoomed-in views, and error maps on our raw dataset. T1-FLAIR MR images are used to help the reconstruction of T2-weighted MRI with random under-sampling pattern at 8× acceleration ratio.

our proposed method brings in more details, like the S-shaped dark signal in yellow circles.

### C. Ablation Study

In this section, we analyze the effects of our hybrid supervision over spatial alignment network (Section IV-C1), the impact of spatial misalignment upon the image quality (Section IV-C2), and computational complexity (Section IV-C3).

1) *Hybrid supervision*: Our hybrid supervision over the spatial alignment network, which consists of a common reconstruction loss  $\mathcal{L}_{\text{rec}}$  and a direct cross-modality-synthesis-based registration loss  $\mathcal{L}_{\text{reg}}$ , is of vital importance to the network optimization. To prove the necessity and superiority of such hybrid supervision, we perform experiments with the spatial alignment network  $T_{\omega}$  and the reconstruction network  $R_{\theta}$  optimized with solely the reconstruction loss  $\mathcal{L}_{\text{rec}}$  (“Rec” in

Fig. 6, 7, and 8) or the registration loss  $\mathcal{L}_{\text{reg}}$  (“Reg” in Fig. 6, 7, and 8). For training with the reconstruction loss  $\mathcal{L}_{\text{rec}}$  only (“Rec”), we have disabled the registration loss  $\mathcal{L}_{\text{reg}}$  and the adversarial training  $\mathcal{L}_{\text{adv}}$ . For training with the reconstruction loss  $\mathcal{L}_{\text{reg}}$  only (“Reg”), first our spatial alignment network  $T_{\omega}$  is optimized without  $\mathcal{L}_{\text{rec}}$ , and then we freeze  $T_{\omega}$  to train the reconstruction network  $R_{\theta}$  with  $\mathcal{L}_{\text{rec}}$ .

Fig. 6 quantitatively demonstrates the superiority of our hybrid supervision and Fig. 7 supports its robustness on the DICOM dataset. In Fig. 6, the performances of different methods, settings, and metrics are presented in box plots, with black bars and diamonds showing the median and mean values. The box plots from left to right are for single-modal reconstruction (“Single-Modal”, pink), multi-modal reconstruction without spatial alignment network (“Multi-Modal”, blue), and multi-modal reconstruction with spatial alignment network trained with solely  $\mathcal{L}_{\text{reg}}$  (“Reg”, green), solely  $\mathcal{L}_{\text{rec}}$  (“Rec”, purple), or our proposed hybrid supervision (“Proposed”, yellow). Comparing single-modal reconstruction (“Single-Modal”) with multi-modal reconstruction (“Multi-Modal”, “Rec”, “Reg”, and “Proposed”), the latter ones are always better than the MR images reconstructed without a reference modality. Among multi-modal reconstruction methods, the spatial alignment network trained with solely  $\mathcal{L}_{\text{reg}}$  (“Reg”) or  $\mathcal{L}_{\text{rec}}$  (“Rec”) not necessarily benefits multi-modal reconstruction (“Multi-Modal”) (e.g. SSIM of 4× random under-sampling pattern), while our hybrid supervision (“Proposed”) can always perform better than all other methods. Fig. 7 plots the distribution of the subject-wise performance gains brought by the spatial alignment network, which are optimized with different loss functions (“Rec”, “Reg”, and “Proposed”) and compared to multi-modal reconstruction without the spatial alignment network (“Multi-Modal”). It reveals that the optimization with solely  $\mathcal{L}_{\text{reg}}$  (“Reg”) or  $\mathcal{L}_{\text{rec}}$  (“Rec”) is suboptimal and somehow unstable where the portion of the subjects with positive performance gain varies from 20% to 100%. For example, with 4× acceleration, random under-sampling pattern, and SSIM metric, the performance improvement brought by spatial alignment network trained with the “Rec” strategy is negative for most of the subjects, which is absolutely not acceptable. On the contrary, the spatial alignment network trained with hybrid supervision (“Proposed”) not only performs better than other optimization strategies (“Reg” and “Reg”) but also keeps very robust where over 98% subjects can benefit.

It is also necessary to explore the displacement fields generated by the spatial alignment network. Fig. 8 visualizes the estimated displacement fields and the aligned reference images. The displacements are amplified for a factor of 4 and rendered in blue arrows for a clear illustration. The two rows at the bottom are the fully-sampled target images and the ground-truth reference modality in checkerboard visualization. In the zoomed-in views (last row), the spatial misalignment between the two modalities is clearly visible, in that the boundary of the skull is mismatched (pointed by green arrows) and the discontinuity also exists in the brain center-line (pointed by red arrows). In both “Reg” and “Proposed” particularly, the reference image can be well aligned with the target modality, while “Rec” is less accurate in aligning brain center-lines



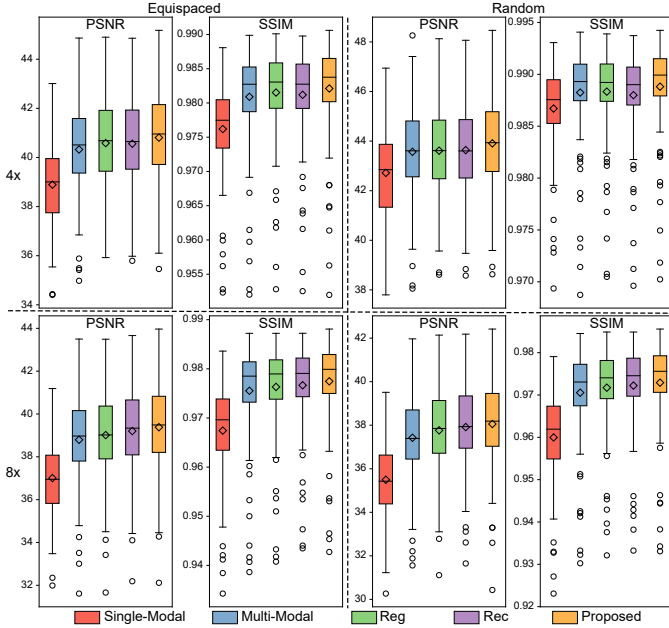


Fig. 6. Quantitative comparison of MRI reconstruction (in PSNR/SSIM) with different methods and loss functions on the DICOM dataset. In each box plot, the average value is marked with the diamond symbol.

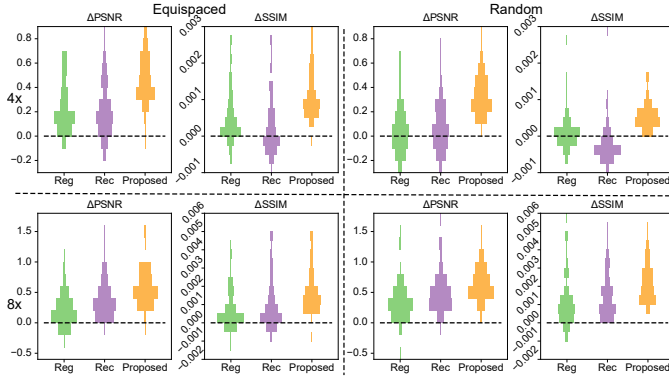


Fig. 7. Performance improvement (in PSNR/SSIM) from the spatial alignment network with different optimization strategies over multi-modal reconstruction without spatial alignment on the DICOM dataset.

(pointed by red arrows as in the last row of the figure). The comparisons underscore our argument that the long-way back-propagated from the reconstruction loss can be insufficient to optimize the spatial alignment network. We also note that, given the example in Fig. 8, the spatial misalignment appears to be subtle rotation in the anti-clockwise direction, which can be attributed to the unexpected motion of the subject.

2) *Degree of Spatial Misalignment*: Multi-modal reconstruction assisted with the spatial alignment network is more robust to different degrees of spatial misalignment. To prove this, we simulate different degrees of spatial misalignment to our DICOM dataset and then evaluate the reconstruction methods optimized in Section IV-A. The simulated spatial misalignment is similar to data augmentation, including random rotation ( $[-0.01\pi\sigma, 0.01\pi\sigma]$ ), translation ( $[-0.05N\sigma, 0.05N\sigma]$ ), and deformation field bicubically interpolated from  $9 \times 9$  control-points (with displacements uniformly sampled within

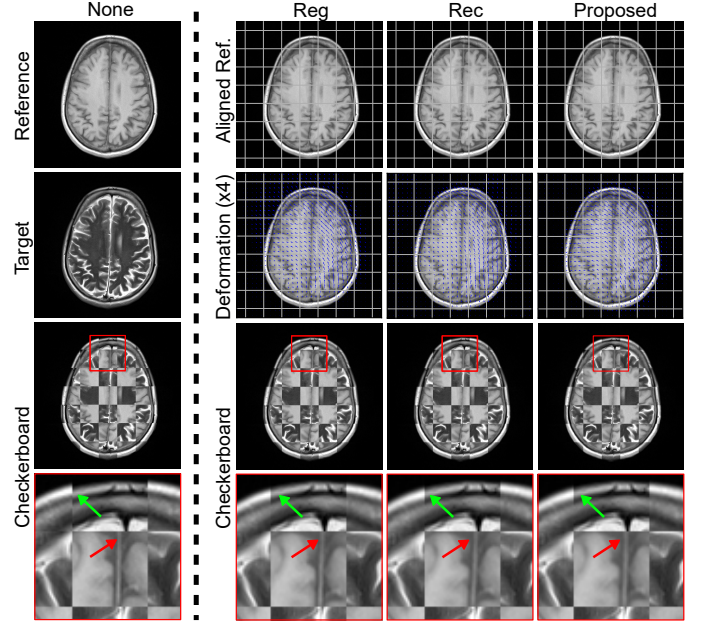


Fig. 8. Effects of the spatial alignment network. The first row shows the original reference images (first column) and the warped ones with different optimization strategies (last three columns). In the second row, the first column is the fully-sampled target, and the rest columns are the deformation fields. The third row contains checkerboard visualizations of the spatial misalignment between the target and the original/warped reference images, the zoomed-in views of which are presented in the last row. The results of the random under-sampling pattern at  $8\times$  acceleration ratio are compared. Note the displacement fields are amplified by four times for better visualization.

$[-0.02N\sigma, 0.02N\sigma]$  in both directions. Here  $N$  is the size of the MR images and  $\sigma$  is the factor controlling the degree of spatial misalignment). Also, note that the simulated spatial misalignment applies to the reference images only, while data augmentation warps both reference and target images. Fig. 9 compares the reconstruction performances (left y-axes) and performance gains of the proposed method (right y-axes) with varying degrees of simulated spatial misalignment (x-axes). The “Proposed” method is plotted in orange triangles, the “Multi-Modal” reconstruction without the spatial alignment is plotted in blue circles, the magenta rectangles are for the performance improvement brought by the spatial alignment network (“Difference”), and the pink dashed lines are for the “Single-Modal” reconstruction. The curves in Fig. 9 clearly indicate that the performance of both “Proposed” and “Multi-Modal” monotonically drops with larger spatial misalignment. It is also interesting to see that, with spatial misalignment increasing, the “Difference”, or the performance improvement between “Proposed” and “Multi-Modal”, first increase and then decreases.

3) *Computational Complexity Comparison*: Other than accuracy, computational complexity is also important. Table III lists four important measures of the complexity, including the number of parameters, the amount of multiply-accumulates (MACs), the inference time and memory requirement of  $G_\rho$ ,  $D_\gamma$ ,  $T_\omega$  and  $R_\theta$ . More specifically, MACs are measured with the ptflops<sup>2</sup> tool, while the inference time and the memory

<sup>2</sup><https://github.com/sovrasov/flops-counter.pytorch>

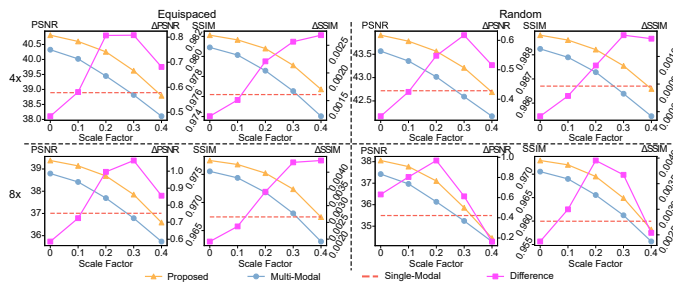


Fig. 9. Quantitative comparison of multi-modal MRI reconstruction with varying degrees of simulated spatial misalignment. For all subplots, left y-axes are for reconstruction performances (“Proposed”, “Multi-Modal”, and “Single-Modal”) while the right y-axes are for the “Difference” between “Proposed” and “Multi-Modal”.

TABLE III

COMPUTATIONAL COMPLEXITY OF NEURAL NETWORKS USED IN OUR PROPOSED METHOD.

Coils & Size	Complexity	$G_\rho$	$D_\gamma$	$T_\omega$	$R_\theta$
1-Coil MRI	MACs (G)	88.33	17.63	12.80	55.95
	Parameters (M)	22.88	3.51	0.72	20.12
	Time (ms)	16.01	3.06	4.27	31.61
320 × 320	Memory (MiB)	179.63	52.39	78.06	42.13
	MACs (G)	88.33	17.63	14.15	87.29
	Parameters (M)	22.88	3.51	0.73	20.12
24-Coil MRI	Time (ms)	15.99	3.06	4.49	69.66
	Memory (MiB)	179.74	52.39	96.03	112.89

footprint are measured on an Nvidia TITAN RTX GPU. For all networks, the computational complexity with both DICOM and raw datasets is measured. From Table III, it is obvious that our cross-modality synthesis network  $G_\rho$  and the reconstruction network  $R_\theta$  cost much more than the other two networks. Moreover, considering that  $G_\rho$  is only used in the offline training, our spatial alignment network  $T_\omega$ , which is an ultra-light module, is the only overhead compared with the multi-modal MRI reconstruction method without spatially aligning the reference image.

## V. DISCUSSION AND CONCLUSION

In this manuscript, to deal with the subtle spatial misalignment between MRI sequences, which is unfortunately prevalent even in the same study, we propose to explicitly align the reference modality with the target modality, and feed them together to the deep network for the reconstruction of the target. More specifically, the spatial alignment network takes fully-sampled reference MRI and under-sampled target image as the input and outputs the displacement field to align the reference modality. Also, a hybrid optimization strategy is proposed to provide strong training supervision for the spatial alignment network. Experiments on both the DICOM and raw MRI datasets demonstrate that the spatial alignment network not only improves overall reconstruction performance but also is robust to bring performance gain to almost all subjects. The proposed spatial alignment network is flexible, and theoretically, it can be plug-in into any multi-modal reconstruction network.

We believe that the spatial alignment network is an important yet missing component towards practical multi-modal

reconstruction. Further research directions include extending our solution to more organs and 3D MR images, while in this manuscript we only work on 2D cases due to large slice spacing. Also, it is a promising way to alternatively align different sequences and reconstruct MRI, which is suitable to work with state-of-the-art unrolled reconstruction methods. Finally, as a general plug-and-play module, the spatial alignment network has great potential in improving the performance of joint reconstruction with multiple ( $\geq 3$ ) MRI sequences or joint k-space under-sampling pattern learning.

## REFERENCES

- [1] K. P. Pruessmann, M. Weiger, M. B. Scheidegger, and P. Boesiger, “SENSE: Sensitivity encoding for fast MRI,” *Magnetic Resonance in Medicine*, vol. 42, no. 5, pp. 952–962, 1999.
- [2] M. A. Griswold, P. M. Jakob, R. M. Heidemann, M. Nittka, V. Jellus, J. Wang, B. Kiefer, and A. Haase, “Generalized autocalibrating partially parallel acquisitions (GRAPPA),” *Magnetic Resonance in Medicine*, vol. 47, no. 6, pp. 1202–1210, 2002.
- [3] M. Lustig, D. Donoho, and J. M. Pauly, “Sparse MRI: The application of compressed sensing for rapid MR imaging,” *Magnetic Resonance in Medicine*, vol. 58, no. 6, pp. 1182–1195, 2007.
- [4] L. Xiang, Y. Chen, W. Chang, Y. Zhan, W. Lin, Q. Wang, and D. Shen, “Ultra-Fast T2-Weighted MR Reconstruction Using Complementary T1-Weighted Information,” in *Medical Image Computing and Computer Assisted Intervention - MICCAI 2018*, ser. Lecture Notes in Computer Science, A. F. Frangi, J. A. Schnabel, C. Davatzikos, C. Alberola-Lopez, and G. Fichtinger, Eds. Cham: Springer International Publishing, 2018, pp. 215–223.
- [5] K. H. Kim, W.-J. Do, and S.-H. Park, “Improving resolution of MR images with an adversarial network incorporating images with different contrast,” *Medical Physics*, vol. 45, no. 7, pp. 3120–3131, 2018.
- [6] Z. Lai, X. Qu, H. Lu, X. Peng, D. Guo, Y. Yang, G. Guo, and Z. Chen, “Sparse MRI reconstruction using multi-contrast image guided graph representation,” *Magnetic Resonance Imaging*, vol. 43, pp. 95–104, Nov. 2017.
- [7] L. Xiang, Y. Chen, W. Chang, Y. Zhan, W. Lin, Q. Wang, and D. Shen, “Deep-Learning-Based Multi-Modal Fusion for Fast MR Reconstruction,” *IEEE Transactions on Biomedical Engineering*, vol. 66, no. 7, pp. 2105–2114, Jul. 2019.
- [8] B. Zhou and S. K. Zhou, “DuDoRNet: Learning a Dual-Domain Recurrent Network for Fast MRI Reconstruction With Deep T1 Prior,” in *2020 IEEE/CVF Conference on Computer Vision and Pattern Recognition (CVPR)*, Jun. 2020, pp. 4272–4281, iSSN: 2575-7075.
- [9] Q. Lyu, H. Shan, C. Steber, C. Helis, C. Whitlow, M. Chan, and G. Wang, “Multi-Contrast Super-Resolution MRI Through a Progressive Network,” *IEEE Transactions on Medical Imaging*, vol. 39, no. 9, pp. 2738–2749, Sep. 2020, conference Name: IEEE Transactions on Medical Imaging.
- [10] S. U. Dar, M. Yurt, M. Shahdloo, M. E. Ildiz, B. Tinaz, and T. Cukur, “Prior-Guided Image Reconstruction for Accelerated Multi-Contrast MRI via Generative Adversarial Networks,” *IEEE Journal of Selected Topics in Signal Processing*, vol. 14, no. 6, pp. 1072–1087, Oct. 2020.
- [11] L. Sun, Z. Fan, X. Fu, Y. Huang, X. Ding, and J. Paisley, “A Deep Information Sharing Network for Multi-Contrast Compressed Sensing MRI Reconstruction,” *IEEE Transactions on Image Processing*, vol. 28, no. 12, pp. 6141–6153, Dec. 2019, conference Name: IEEE Transactions on Image Processing.
- [12] D. L. Donoho, “Compressed sensing,” *IEEE Transactions on Information Theory*, vol. 52, no. 4, pp. 1289–1306, Apr. 2006.
- [13] S. Wang, Z. Su, L. Ying, X. Peng, S. Zhu, F. Liang, D. Feng, and D. Liang, “Accelerating magnetic resonance imaging via deep learning,” in *2016 IEEE 13th International Symposium on Biomedical Imaging (ISBI)*, Apr. 2016, pp. 514–517, iSSN: 1945-8452.
- [14] J. Schlemper, J. Caballero, J. V. Hajnal, A. N. Price, and D. Rueckert, “A Deep Cascade of Convolutional Neural Networks for Dynamic MR Image Reconstruction,” *IEEE Transactions on Medical Imaging*, vol. 37, no. 2, pp. 491–503, Feb. 2018.
- [15] C. Qin, J. Schlemper, J. Caballero, A. N. Price, J. V. Hajnal, and D. Rueckert, “Convolutional Recurrent Neural Networks for Dynamic MR Image Reconstruction,” *IEEE Transactions on Medical Imaging*, vol. 38, no. 1, pp. 280–290, Jan. 2019.

- [16] Y. Han, L. Sunwoo, and J. C. Ye, “k-Space Deep Learning for Accelerated MRI,” *IEEE Transactions on Medical Imaging*, vol. 39, no. 2, pp. 377–386, Feb. 2020.
- [17] Y. Zhang, P.-T. Yap, L. Qu, J.-Z. Cheng, and D. Shen, “Dual-domain convolutional neural networks for improving structural information in 3 T MRI,” *Magnetic Resonance Imaging*, vol. 64, pp. 90–100, Dec. 2019.
- [18] B. Zhu, J. Z. Liu, S. F. Cauley, B. R. Rosen, and M. S. Rosen, “Image reconstruction by domain-transform manifold learning,” *Nature*, vol. 555, no. 7697, pp. 487–492, Mar. 2018.
- [19] J. Zbontar, F. Knoll, A. Sriram, T. Murrell, Z. Huang, M. J. Muckley, A. Defazio, R. Stern, P. Johnson, M. Bruno, M. Parente, K. J. Geras, J. Katsnelson, H. Chandarana, Z. Zhang, M. Drozdal, A. Romero, M. Rabbat, P. Vincent, N. Yakubova, J. Pinkerton, D. Wang, E. Owens, C. L. Zitnick, M. P. Recht, D. K. Sodickson, and Y. W. Lui, “fastMRI: An Open Dataset and Benchmarks for Accelerated MRI,” *arXiv:1811.08839 [physics, stat]*, Dec. 2019, arXiv: 1811.08839.
- [20] F. Knoll, J. Zbontar, A. Sriram, M. J. Muckley, M. Bruno, A. Defazio, M. Parente, K. J. Geras, J. Katsnelson, H. Chandarana, Z. Zhang, M. Drozdal, A. Romero, M. Rabbat, P. Vincent, J. Pinkerton, D. Wang, N. Yakubova, E. Owens, C. L. Zitnick, M. P. Recht, D. K. Sodickson, and Y. W. Lui, “fastMRI: A Publicly Available Raw k-Space and DICOM Dataset of Knee Images for Accelerated MR Image Reconstruction Using Machine Learning,” *Radiology: Artificial Intelligence*, vol. 2, no. 1, p. e190007, Jan. 2020.
- [21] F. Knoll, T. Murrell, A. Sriram, N. Yakubova, J. Zbontar, M. Rabbat, A. Defazio, M. J. Muckley, D. K. Sodickson, C. L. Zitnick *et al.*, “Advancing machine learning for mr image reconstruction with an open competition: Overview of the 2019 fastmri challenge,” *Magnetic resonance in medicine*, vol. 84, no. 6, pp. 3054–3070, 2020.
- [22] M. J. Muckley, B. Riemenschneider, A. Radmanesh, S. Kim, G. Jeong, J. Ko, Y. Jun, H. Shin, D. Hwang, M. Mostapha *et al.*, “Results of the 2020 fastmri challenge for machine learning mr image reconstruction,” *IEEE transactions on medical imaging*, vol. 40, no. 9, pp. 2306–2317, 2021.
- [23] R. Souza, Y. Beauferris, W. Loos, R. M. Lebel, and R. Frayne, “Enhanced Deep-Learning-Based Magnetic Resonance Image Reconstruction by Leveraging Prior Subject-Specific Brain Imaging: Proof-of-Concept Using a Cohort of Presumed Normal Subjects,” *IEEE Journal of Selected Topics in Signal Processing*, vol. 14, no. 6, pp. 1126–1136, Oct. 2020.
- [24] L. Weizman, Y. C. Eldar, and D. B. Bashat, “Compressed sensing for longitudinal MRI: An adaptive-weighted approach,” *Medical Physics*, vol. 42, no. 9, pp. 5195–5208, 2015.
- [25] —, “Reference-based MRI,” *Medical Physics*, vol. 43, no. 10, pp. 5357–5369, 2016.
- [26] A. Hirabayashi, N. Inamuro, K. Mimura, T. Kurihara, and T. Homma, “Compressed sensing MRI using sparsity induced from adjacent slice similarity,” in *2015 International Conference on Sampling Theory and Applications (SampTA)*, May 2015, pp. 287–291.
- [27] A. Majumdar and R. K. Ward, “Joint reconstruction of multiecho MR images using correlated sparsity,” *Magnetic Resonance Imaging*, vol. 29, no. 7, pp. 899–906, Sep. 2011.
- [28] J. Huang, C. Chen, and L. Axel, “Fast multi-contrast MRI reconstruction,” *Magnetic Resonance Imaging*, vol. 32, no. 10, pp. 1344–1352, Dec. 2014.
- [29] P. Song, L. Weizman, J. F. C. Mota, Y. C. Eldar, and M. R. D. Rodrigues, “Coupled Dictionary Learning for Multi-Contrast MRI Reconstruction,” *IEEE Transactions on Medical Imaging*, vol. 39, no. 3, pp. 621–633, Mar. 2020.
- [30] L. Xiang, Y. Qiao, D. Nie, L. An, W. Lin, Q. Wang, and D. Shen, “Deep auto-context convolutional neural networks for standard-dose PET image estimation from low-dose PET/MRI,” *Neurocomputing*, vol. 267, pp. 406–416, Dec. 2003.
- [31] B. B. Avants, C. L. Epstein, M. Grossman, and J. C. Gee, “Symmetric diffeomorphic image registration with cross-correlation: Evaluating automated labeling of elderly and neurodegenerative brain,” *Medical Image Analysis*, vol. 12, no. 1, pp. 26–41, Feb. 2008.
- [32] J. P. Thirion, “Image matching as a diffusion process: an analogy with Maxwell’s demons,” *Medical Image Analysis*, vol. 2, no. 3, pp. 243–260, Sep. 1998.
- [33] T. Vercauteren, X. Pennec, A. Perchant, and N. Ayache, “Diffeomorphic demons: Efficient non-parametric image registration,” *NeuroImage*, vol. 45, no. 1, Supplement 1, pp. S61–S72, Mar. 2009.
- [34] P. Hellier, J. Ashburner, I. Corouge, C. Barillot, and K. J. Friston, “Inter-subject Registration of Functional and Anatomical Data Using SPM,” in *Medical Image Computing and Computer-Assisted Intervention - MICCAI 2002*, ser. Lecture Notes in Computer Science, T. Dohi and R. Kikinis, Eds. Berlin, Heidelberg: Springer, 2002, pp. 590–597.
- [35] X. Yang, R. Kwitt, M. Styner, and M. Niethammer, “Quicksilver: Fast predictive image registration - A deep learning approach,” *NeuroImage*, vol. 158, pp. 378–396, Sep. 2017.
- [36] G. Balakrishnan, A. Zhao, M. R. Sabuncu, A. V. Dalca, and J. Guttag, “An Unsupervised Learning Model for Deformable Medical Image Registration,” in *2018 IEEE/CVF Conference on Computer Vision and Pattern Recognition*, Jun. 2018, pp. 9252–9260.
- [37] T. Küstner, J. Pan, H. Qi, G. Cruz, C. Gilliam, T. Blu, B. Yang, S. Gatidis, R. Botnar, and C. Prieto, “LAPNet: Non-Rigid Registration Derived in k-Space for Magnetic Resonance Imaging,” *IEEE Transactions on Medical Imaging*, vol. 40, no. 12, pp. 3686–3697, Dec. 2021, conference Name: IEEE Transactions on Medical Imaging.
- [38] P. Thevenaz and M. Unser, “Optimization of mutual information for multiresolution image registration,” *IEEE Transactions on Image Processing*, vol. 9, no. 12, pp. 2083–2099, Dec. 2000.
- [39] D. Mattes, D. R. Haynor, H. Vesselle, T. K. Lewellen, and W. Eubank, “PET-CT image registration in the chest using free-form deformations,” *IEEE Transactions on Medical Imaging*, vol. 22, no. 1, pp. 120–128, Jan. 2003.
- [40] S. M. Smith, M. Jenkinson, M. W. Woolrich, C. F. Beckmann, T. E. J. Behrens, H. Johansen-Berg, P. R. Bannister, M. De Luca, I. Drobnjak, D. E. Flitney, R. K. Niazy, J. Saunders, J. Vickers, Y. Zhang, N. De Stefano, J. M. Brady, and P. M. Matthews, “Advances in functional and structural MR image analysis and implementation as FSL,” *NeuroImage*, vol. 23, pp. S208–S219, Jan. 2004.
- [41] M. P. Heinrich, M. Jenkinson, M. Bhushan, T. Martin, F. V. Gleeson, S. M. Brady, and J. A. Schnabel, “MIND: Modality independent neighbourhood descriptor for multi-modal deformable registration,” *Medical Image Analysis*, vol. 16, no. 7, pp. 1423–1435, Oct. 2012.
- [42] J. Fan, X. Cao, Q. Wang, P.-T. Yap, and D. Shen, “Adversarial learning for mono- or multi-modal registration,” *Medical Image Analysis*, vol. 58, p. 101545, Dec. 2019.
- [43] X. Cao, J. Yang, Y. Gao, Q. Wang, and D. Shen, “Region-adaptive deformable registration of ct/mri pelvic images via learning-based image synthesis,” *IEEE Transactions on Image Processing*, vol. 27, no. 7, pp. 3500–3512, 2018.
- [44] M. Arar, Y. Ginger, D. Danon, A. H. Bermanno, and D. Cohen-Or, “Unsupervised Multi-Modal Image Registration via Geometry Preserving Image-to-Image Translation,” in *2020 IEEE/CVF Conference on Computer Vision and Pattern Recognition (CVPR)*, Jun. 2020, pp. 13 407–13 416, iSSN: 2575-7075.
- [45] A. Sriram, J. Zbontar, T. Murrell, A. Defazio, C. L. Zitnick, N. Yakubova, F. Knoll, and P. Johnson, “End-to-End Variational Networks for Accelerated MRI Reconstruction,” in *Medical Image Computing and Computer Assisted Intervention - MICCAI 2020*, A. L. Martel, P. Abolmaesumi, D. Stoyanov, D. Mateus, M. A. Zuluaga, S. K. Zhou, D. Racoceanu, and L. Joskowicz, Eds. Springer International Publishing, 2020, pp. 64–73.
- [46] Z. Wang, E. P. Simoncelli, and A. C. Bovik, “Multiscale structural similarity for image quality assessment,” in *The Thirty-Seventh Asilomar Conference on Signals, Systems Computers, 2003*, vol. 2, Nov. 2003, pp. 1398–1402 Vol.2.
- [47] T. Miyato, T. Kataoka, M. Koyama, and Y. Yoshida, “Spectral Normalization for Generative Adversarial Networks,” in *International Conference on Learning Representations*, Feb. 2018.
- [48] O. Ronneberger, P. Fischer, and T. Brox, “U-net: Convolutional networks for biomedical image segmentation,” in *International Conference on Medical image computing and computer-assisted intervention*. Springer, 2015, pp. 234–241.
- [49] P. Isola, J.-Y. Zhu, T. Zhou, and A. A. Efros, “Image-to-image translation with conditional adversarial networks,” in *Proceedings of the IEEE conference on computer vision and pattern recognition*, 2017, pp. 1125–1134.
- [50] S. Ioffe and C. Szegedy, “Batch normalization: Accelerating deep network training by reducing internal covariate shift,” in *International conference on machine learning*. PMLR, 2015, pp. 448–456.
- [51] A. Paszke, S. Gross, F. Massa, A. Lerer, J. Bradbury, G. Chanan, T. Killeen, Z. Lin, N. Gimelshein, L. Antiga *et al.*, “Pytorch: An imperative style, high-performance deep learning library,” *Advances in neural information processing systems*, vol. 32, pp. 8026–8037, 2019.
- [52] D. P. Kingma and J. Ba, “Adam: A method for stochastic optimization,” in *ICLR (Poster)*, 2015.